

# Extended Source Effects in Astrometric Gravitational Microlensing

Shude Mao<sup>1\*</sup> Hans J. Witt<sup>2†</sup>

<sup>1</sup>*Max-Planck-Institute für Astrophysik, Karl-Schwarzschild-Strasse 1, 85740 Garching, Germany*

<sup>2</sup>*Astrophysikalisches Institut Potsdam, An der Sternwarte 16, 14482 Potsdam, Germany*

Accepted ..... Received .....; in original form .....

## ABSTRACT

Extended source size effects have been detected in photometric monitoring of gravitational microlensing events. We study similar effects in the centroid motion of an extended source lensed by a point mass. We show that the centroid motion of a source with uniform surface brightness can be obtained analytically. For a source with circularly symmetric limb-darkening profile, the centroid motion can be expressed as a one-dimensional integral, which can be evaluated numerically. We found that when the impact parameter is comparable to the source radius, the centroid motion is significantly modified by the finite source size. In particular, when the impact parameter is smaller than the source radius, the trajectories become clover-leaf like. Such astrometric motions can be detected using space interferometers such as the Space Interferometry Mission. Such measurements offer exciting possibilities of determining stellar parameters such as stellar radius to excellent accuracy.

**Key words:** astrometry – galaxy: halo – gravitational lensing – stars: fundamental parameters

## 1 INTRODUCTION

Gravitational microlensing has produced many interesting scientific returns concerning the Galactic structure, dark matter and variable stars (see Paczyński 1996a for a review). The

\* e-mail: smao@mpa-garching.mpg.de

† e-mail: hwitt@aip.de

current (photometric) observations of microlensing events have one notable shortcoming: from the observed time scale of microlensing event one cannot infer the lens mass and distance, since this measured quantity depends on the lens mass, distances to the lens and the source and the relative lens and source transverse motion. This degeneracy can be partially or even completely removed using some rare microlensing events (e.g., Gould 1996, 1997). A much more general way of lifting the degeneracy is conducting an accurate astrometric program together with the photometric observations (Hosokawa et al. 1993, Høg, Novikov & Polnarev 1995, Miyamoto & Yoshi 1995, and Walker 1995); we refer to such an astrometric experiment as astrometric microlensing. Accurate astrometry can measure the angular Einstein radius and the relative parallax between the lens and source. With these two additional constraints, the lens mass can be determined, even if we have no independent measures of the lens and source distances (Paczynski 1998; Boden, Shao, & Van Buren 1998). This method also opens up the possibility of measuring the mass of nearby high proper-motion stars (Miralda-Escudé 1996, Paczynski 1996b). Boden et al. (1998) showed that the required astrometric accuracy can be reached by ground interferometers soon available on 8-10m class telescopes such as KECK and VLT. The Space Interferometry mission (SIM), to be launched in 2004, offers the best hope for disentangling the lens degeneracy with its global astrometric accuracy of  $\sim \mu\text{as}$ . Ground and space interferometers (for a review see Shao & Colavita 1992) therefore offers exciting possibilities of measuring the mass of lenses, which may turn out to be brown dwarfs, planets etc.

Paczynski (1998) pointed out that, using astrometric observations, it is possible to measure the stellar radius to 1% accuracy for microlensed sources which show finite size effect. The photometric extended source effect has been studied by many workers (Witt & Mao 1994; Gould 1994; Nemiroff & Wickramasinghe 1994). However, up to now, most studies of astrometric microlensing adopt a point source approximation; the only exception is Walker (1995), who briefly discussed the astrometric extended source effect. Since the photometric extended source effects have already been detected for several sources (95-BLG-30, Alcock et al. 1997; 97-BLG-28, Albrow et al. 1998 and 97-BLG-56) and in light of the possibility of measuring stellar radii and other stellar parameters to excellent accuracy, we study the astrometric extended source effects in detail. In §2, we first derive analytical expressions for the centroid motion for a source with uniform surface brightness. The centroid motion for sources with (realistic) limb-darkening profiles are then simplified into a one-dimensional integral, which can be computed easily numerically. In §3, we discuss briefly our results.

Throughout this paper, we ignore parallactic effects, since this subject has been covered in detail by other authors (e.g., Hosokawa et al. 1993, Høg et al. 1995, Miyamoto & Yoshi 1995).

## 2 RESULTS

We shall work in angular coordinates and all angles are normalized to the Einstein ring angular scale given by (e.g., Schneider, Ehlers, & Falco 1992; Paczyński 1996a)

$$\theta_E = 0.9 \text{ mas} \left( \frac{M}{M_\odot} \right)^{1/2} \left( \frac{10 \text{ kpc}}{D} \right)^{1/2}, D \equiv \frac{D_d D_s}{D_s - D_d}, \quad (1)$$

where  $D_s$ ,  $D_d$ , and  $M$  are the distance to the source and the distance to the lens (deflector), and the lens mass, respectively. For convenience, we first choose a coordinate system centered on the lens but later (for observation considerations) transform the results into a system where the source is at the origin (see eq. [15]). We use complex quantities to obtain a more compact representation of the lens equation (Witt 1990). In this formalism, the lens equation is simply

$$\zeta = z - \frac{1}{\bar{z}}, \quad (2)$$

where  $z = x + iy$  are the coordinates in the deflector plane,  $\zeta = \xi + i\eta$  the coordinates in the source plane, and  $\bar{z}$  denotes the complex conjugate of  $z$ . Again, both  $z$  and  $\zeta$  are normalized to  $\theta_E$  given by Equation (1). (Note that for the case where  $z$  and  $\zeta$  are expressed in length units we obtain a different normalization in each plane (cf. Witt & Mao 1994)).

Eq. (2) can be easily solved to yield two image positions, which are denoted by subscripts + and - indicating their respective positive and negative parities (Witt & Mao 1994):

$$z_{+,-} = \frac{\zeta}{2} \left[ 1 \pm \sqrt{1 + \frac{4}{\zeta \bar{\zeta}}} \right]. \quad (3)$$

The separation between the images are comparable to  $\theta_E$  when the distance between the lens and source is a few Einstein radii; for microlensing in the local group,  $D \sim 10$  kpc, the separation is  $\sim$  mas, too small to be resolved. Therefore we can only observe the motion of the centroid of light for these two images. For a point source, the centroid motion forms an ellipse in a coordinate system where the unperturbed source is at the origin (e.g., Walker 1995; see eq. [16] below). In the next subsections, we first study the centroid motion for extended sources with uniform surface brightness and then for sources with more realistic profiles.

## 2.1 Analytical Results for a Uniform Source

Let us now consider a circular source with radius  $r$  and constant surface brightness. The boundary of the circular source is simply described by  $\zeta(\varphi) = \zeta_0 + re^{i\varphi}$ . Using eq. (3), we obtain a parametric representation for the image contours:

$$\begin{aligned} z_{+,-}(\varphi) &= \frac{\zeta_0 + re^{i\varphi}}{2} \left[ 1 \pm \sqrt{1 + \frac{4}{g(\varphi)}} \right] \\ &= x_{+,-}(\varphi) + iy_{+,-}(\varphi), \quad 0 \leq \varphi \leq 2\pi, \end{aligned} \quad (4)$$

where we have assumed (without losing generality) that  $\zeta_0$  is on the positive real  $\xi$ -axis, and  $g(\varphi) = r^2 + \zeta_0^2 + 2r\zeta_0 \cos \varphi$ .

Since lensing conserves surface brightness, the magnification of a circular source with uniform surface brightness is just given by the ratio of the area of the images to the area of the source:

$$\mu_{\text{tot}} = \frac{1}{\pi r^2} \int_0^{2\pi} \left[ -y_+(\varphi) \frac{dx_+(\varphi)}{d\varphi} + y_-(\varphi) \frac{dx_-(\varphi)}{d\varphi} \right] d\varphi \quad . \quad (5)$$

Note that the minus sign results from the fact that when  $\varphi$  changes from 0 to  $2\pi$ , the contour for the image with positive parity moves counter-clockwise whereas that with negative parity moves clockwise. This integral can be evaluated analytically; the results have been presented in Witt & Mao (1994). They are given below for completeness and comparison purposes.

We can now calculate the centroid of light by weighting the image positions with magnification. For a circular source we obtain

$$\Delta\theta_x = \frac{1}{\pi r^2 \mu_{\text{tot}}} \int_0^{2\pi} \left[ -x_+(\varphi)y_+(\varphi) \frac{dx_+(\varphi)}{d\varphi} + x_-(\varphi)y_-(\varphi) \frac{dx_-(\varphi)}{d\varphi} \right] d\varphi \quad . \quad (6)$$

Obviously we have  $\Delta\theta_y = 0$  because of the reflection symmetry with respect to the  $x$ -axis.

After a partial integration the integral becomes

$$\Delta\theta_x = \frac{1}{3\pi r \mu_{\text{tot}}} \int_0^{2\pi} (\zeta_0 + r \cos \varphi)(r + \zeta_0 \cos \varphi) \frac{1 + g(\varphi)}{g(\varphi)} \sqrt{1 + \frac{4}{g(\varphi)}} d\varphi, \quad (7)$$

where  $g(\varphi)$  is defined under eq. (4). After some tedious algebra we find, similar to the case of magnification for a uniform source, the integral can be simplified into two expressions, one for the special case of  $\zeta_0 = r$  and one for the more general case when  $\zeta_0 \neq r$ .

For  $\zeta_0 \neq r$ , one finds

$$\Delta\theta_x = \frac{1}{4\pi r^2 \zeta_0 \mu_{\text{tot}} \sqrt{4 + (\zeta_0 - r)^2}} \left[ a_1 F\left(\frac{\pi}{2}, k\right) + a_2 E\left(\frac{\pi}{2}, k\right) + a_3 \Pi\left(\frac{\pi}{2}, n, k\right) \right], \quad (8)$$

$$\mu_{\text{tot}} = \frac{1}{2\pi r^2 \sqrt{4 + (\zeta_0 - r)^2}} \left[ b_1 F\left(\frac{\pi}{2}, k\right) + b_2 E\left(\frac{\pi}{2}, k\right) + b_3 \Pi\left(\frac{\pi}{2}, n, k\right) \right], \quad (9)$$

where  $F, E, \Pi$  are respectively the first, second and third kind of elliptic integrals as defined in Gradshteyn & Ryzhik (1980), and

$$n = \frac{4\zeta_0 r}{(\zeta_0 + r)^2} \quad \text{and} \quad k = \sqrt{\frac{4n}{4 + (\zeta_0 - r)^2}}. \quad (10)$$

The coefficients are defined as follows

$$a_1 = -(8 + r^2 + \zeta_0^2)(r + \zeta_0)(\zeta_0 - r)^2, \quad b_1 = -(8 - r^2 + \zeta_0^2)(\zeta_0 - r), \quad (11)$$

$$a_2 = (4 + (r - \zeta_0)^2)(r + \zeta_0)(r^2 + \zeta_0^2), \quad b_2 = (4 + (r - \zeta_0)^2)(r + \zeta_0), \quad (12)$$

$$a_3 = 4(2r^2\zeta_0^2 + r^2 + \zeta_0^2)(r - \zeta_0)^2/(r + \zeta_0), \quad b_3 = 4(1 + r^2)(r - \zeta_0)^2/(r + \zeta_0). \quad (13)$$

For  $\zeta_0 = r$ , we obtain

$$\Delta\theta_x = \zeta_0 = r, \quad \mu_{\text{tot}} = \frac{2}{\pi} \left[ \frac{1}{r} + \frac{1 + r^2}{r^2} \arctan r \right]. \quad (14)$$

The centroid motion for this special case is particularly simple. Physically all images of the source boundary fall on two circles: one circle is just the Einstein ring centered at the origin and the other is centered on the source with radius  $(1 + \zeta_0^2)^{1/2}$ . These two circles cross each other at two points,  $(0, 1)$  and  $(0, -1)$ . The contour for the positive parity images rotates counter-clockwise along the two right arc segments and that for the negative parity images rotates clockwise along the two left arc segments. One can show the resulting central shift of these simple configurations is just  $\zeta_0$ .

While it is possible to define the inertial system where the (unperturbed) source is at rest, e.g., by using global astrometry or the positions of nearby stars, it is often difficult or impossible to do so for the lens since it could be dark. It is therefore observationally convenient to express the centroid motion in a system where the (unperturbed) source is at the origin and the lens is moving, say, along the  $x$ -axis. Each trajectory is described by its impact parameter,  $p$ . The centroid position can be obtained as

$$\Delta\theta'_x = x - \Delta\theta_x \frac{x}{\zeta_0}, \quad \Delta\theta'_y = p - \Delta\theta_x \frac{p}{\zeta_0}, \quad (15)$$

where the lens is at  $(x, p)$  and  $\zeta_0 = (x^2 + p^2)^{1/2}$ . Notice it follows from eq. (14) that for  $\zeta_0 = r$ , the centroid shift in this coordinate system is zero. These results for extended sources should be compared with those for a point source (e.g., Walker 1995)

$$\Delta\theta'_x = -\frac{x}{\zeta_0^2 + 2}, \quad \Delta\theta'_y = -\frac{p}{\zeta_0^2 + 2}. \quad (16)$$

When the lens moves from  $-\infty$  to  $+\infty$  parallel to the  $x$ -axis, the centroid motion forms an ellipse with the major axis along the  $x$  direction and the minor axis along the  $y$ -axis.

The (topological) difference between the centroid motion of a point source and that of an extended source is approximately only a function of  $r/p$ . In Fig. 1, we illustrate the difference with one example for a source with  $r = 0.5$ . The centroid motions for four lens trajectories are shown with  $p = +3, +0.8, +0.5$ , and  $+0.1$ , respectively. When the impact parameter is much larger than the source radius (top left), the trajectory of an extended source nearly coincides with that for a point source, as expected intuitively. When the impact parameter decreases to  $\gtrsim r$  (top right), the trajectory begins to deviate from the point source approximation, with the minor axis becoming smaller. For the special case when  $r = p$  (bottom left), the centroid motion goes through the origin; this occurs when the edge of the source touches the lens (cf. eqs. [14] and [15]). As the impact parameter is further reduced, the trajectory becomes clover-leaf like, going through the origin twice (bottom right) since the lens hits the edge of the source twice.

## 2.2 Generalization to Sources with Center-to-Limb Variations

The surface brightness of stars in reality shows center-to-limb variations. In this subsection, we extend our previous results (obtained for constant surface brightness) to such cases. To do this, we first obtain the magnification and centroid shift of an infinitely thin shell at radius  $R$ . We illustrate the derivation by considering the magnification of a shell. The image area of a source with radius  $R$  is given by  $A(R) = \mu_{\text{tot}}(R) \cdot \pi R^2$ , and that of a source with radius  $R + dR$  is given by  $A(R + dR) = \mu_{\text{tot}}(R + dR) \cdot \pi(R + dR)^2$ . The shell magnification is then just the differential image area divided by the shell area, i.e.,  $[A(R + dR) - A(R)]/(2\pi R dR)$ , which yields

$$\mu_s = \frac{1}{2\pi R} \frac{d}{dR} \left( \pi R^2 \mu_{\text{tot}} \right), \quad (17)$$

where the subscript  $s$  indicates the quantities are for a thin shell. Similarly for the centroid shift, we find

$$\Delta\theta_{x,s} = \frac{1}{2\pi R \mu_s} \frac{d}{dR} \left( \pi R^2 \mu_{\text{tot}} \Delta\theta_x \right). \quad (18)$$

Notice the extra magnification factors in  $\Delta\theta_x$  arise because the centroid is weighted by light. For a source with circularly symmetric limb-darkening profile,  $I(R)$ , the magnification and centroid shift are then simply

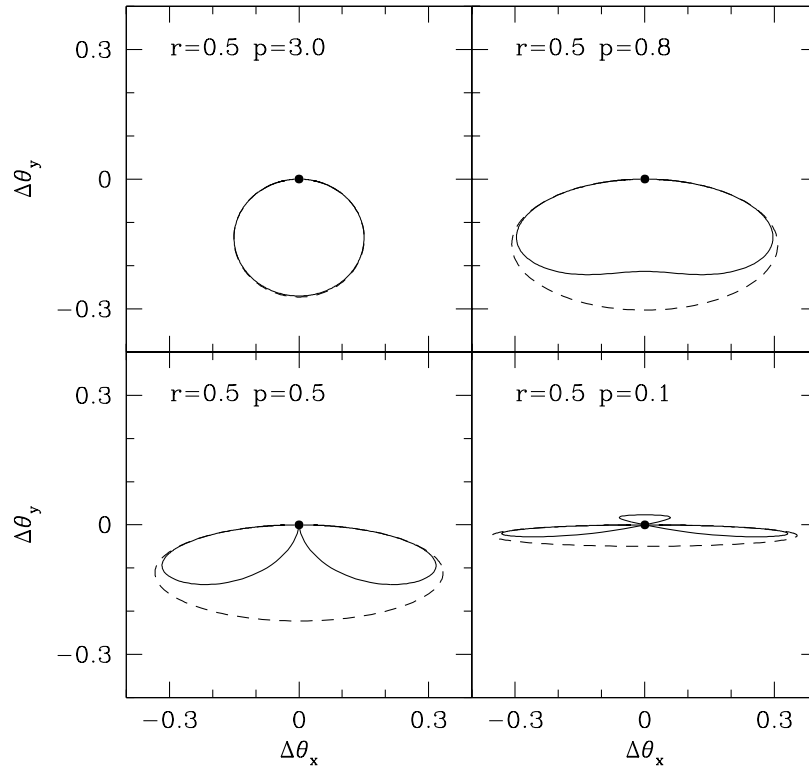


**Figure 1.** Four examples of astrometric trajectories showing finite source size effects. The source size is assumed to be 0.5 Einstein radii ( $r = 0.5$ ). For each example, the black dot marks the source position and the lens is moving from  $-\infty$  to  $\infty$  parallel to the  $x$ -axis. The centroid motion starts at the origin and moves counter-clockwise. The impact parameter ( $p$ ) of the trajectory is shown at the left corner in each panel. For each example, the solid line shows the trajectory that takes into account the finite source size effect while the dashed lines shows that for a point source approximation.

$$\mu_{\text{limb}} = \frac{\int_0^r \mu_s I(R) 2\pi R dR}{\int_0^r I(R) 2\pi R dR}, \quad \Delta\theta_{x,\text{limb}} = \frac{\int_0^r \Delta\theta_{x,s} \mu_s I(R) 2\pi R dR}{\int_0^r \mu_s I(R) 2\pi R dR}. \quad (19)$$

These quantities can be easily evaluated for any limb-darkening profile and transformed into other coordinate systems, e.g., using eq. (15).

Fig. 2 shows the predicted centroid motion for the first microlensing event (95-BLG-30) exhibiting (photometric) extended size effects discovered by the MACHO collaboration (Alcock et al. 1997). The source limb-darkening profile is modelled by

$$\frac{I(R)}{I(0)} = 1 - u_1 - u_2 + u_1 \sqrt{1 - \frac{R^2}{r^2}} + u_2 \left(1 - \frac{R^2}{r^2}\right), \quad (20)$$

with  $u_1 = 0.57$ ,  $u_2 = 0.28$  for the MACHO V band, and  $u_1 = 0.72$ ,  $u_2 = 0.05$  for the MACHO R band. The source radius and impact parameter are found to be  $r = 0.075$ ,  $p = 0.055$ , whereas the Einstein radius angular scale is  $\theta_E = 420 \mu\text{as}$ . For this event, the centroid

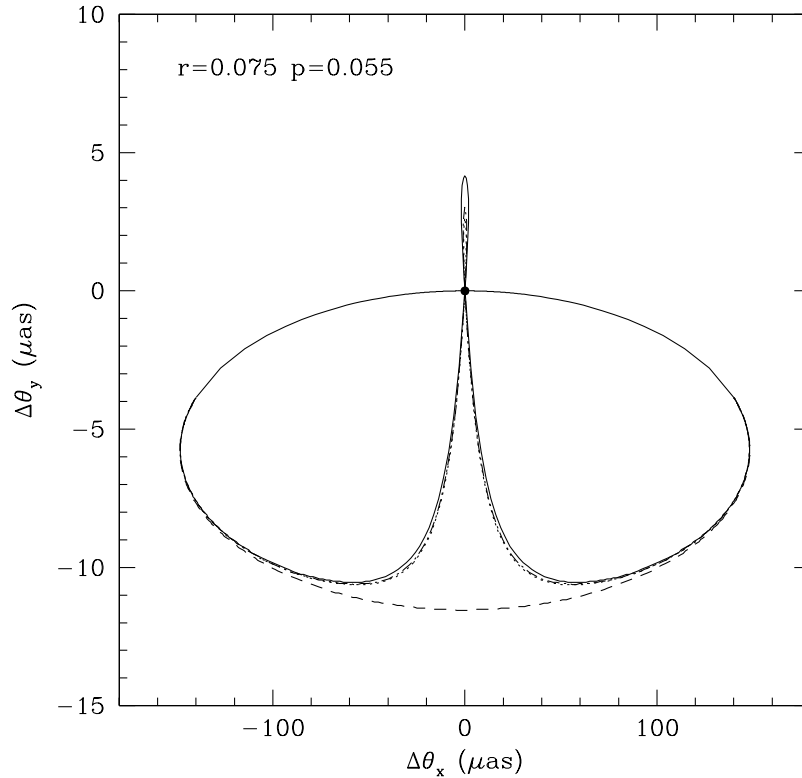


**Figure 2.** Simulated astrometric trajectories for the first microlensing event (95-BLG-30) that shows photometric extended source effects. The parameters used are taken from Alcock et al. (1997). The dashed ellipse is the centroid motion for a point source. The solid line shows the trajectory for a source with constant surface brightness, whereas the dotted and dot-dashed lines show the predictions for the MACHO V and R band, respectively. Note the scales are the two axes are *different* and should be compared with the astrometric accuracy of  $\sim \mu\text{as}$  of the Space Interferometry Mission.

motion displays the clover-leaf like trajectory since we have  $p < r$ . The overall deviations can be easily detected with SIM with its  $\sim \mu\text{as}$  astrometric accuracy. On the other hand, the centroid motions for sources with different profiles are almost the same. We found that in almost all cases, the centroid motion for a source with limb-darkening profiles only show small differences from that for a uniform source. Such small differences will be difficult to detect astrometrically unless we have very dense time samplings.

### 3 DISCUSSION

Extended source effects in photometric monitoring of microlensing events have already been observed for several events. We studied the astrometric signatures of these events in future microlensing experiments using interferometry. For microlensing events that exhibit extended source effects photometrically, the impact parameter is expected to be comparable to the



source radius (e.g., Witt & Mao 1994); for such events, the centroid motion is significantly modified by the finite source size effect and the distinctive clover-leaf features can be easily detected with future interferometers such as SIM (cf. Figs. 1 and 2). These modifications should be taken into account when fitting the centroid motions<sup>‡</sup>. This will add one more parameter to the fitting procedure, but this also means in principle the source size can be obtained independent of photometric observations. We conclude that using astrometric microlensing, it is possible to determine interesting stellar parameters such as stellar radius with  $\sim 1\%$  accuracy (Paczynski 1998). We are anxiously waiting for the arrival of astrometric microlensing.

## ACKNOWLEDGMENTS

We thank Peter Schneider for a careful reading of the manuscript. This work was partially supported by the ‘‘Sonderforschungsbereich 375-95 f ur Astro-Teilchenphysik’’ der Deutschen Forschungsgemeinschaft.

## REFERENCES

- Alcock, C. et al. 1997, preprint: astro-ph/9702199  
 Boden, A. F., Shao, M., & Van Buren, D. 1998, preprint (astro-ph/9802179)  
 Gould, A. 1994, ApJ, 421, L71  
 Gould, A. 1996, PASP, 108, 465  
 Gould, A. 1997, ApJ, 480, 188  
 Gradshteyn, I.S. & Ryzhik, I.M. 1980, Table of Integrals, Series and Products (New York: Academic Press)  
 Hosokawa, M., Ohnishi, K., Fukushima, T. , & Takeuti, M. 1993, A&A, 278, L27  
 H og, E., Novikov, I. D., & Polnarev, A. G. 1995, A&A, 294, 287  
 Miralda-Escud e, J. 1996, ApJ, 470, L113  
 Miyamoto, M. & Yoshii, Y. 1995, AJ, 110, 1427  
 Nemiroff, R.J., Wickramasinghe: 1994, ApJ, 424, L21  
 Paczyński, B. 1996a, ARA&A, 34, 419  
 Paczyński, B. 1996b, AcA, 46, 291  
 Paczyński, B. 1998, ApJ, 494, L23  
 Schneider P., Ehlers J., Falco E. E., 1992, Gravitational Lenses (Springer-Verlag: New York)  
 Shao, M., & Colavita, M. M. 1992, ARA&A, 30, 457  
 Walker, M. A. 1995, ApJ, 453, 37  
 Witt, H.J. 1990, A&A, 236, 311  
 Witt, H.J., & Mao, S. 1994, ApJ, 430, 505

<sup>‡</sup> The software for calculating the centroid motion of an extended source is available at <http://www.mpa-garching.mpg.de/~smao/centroid>

This paper has been produced using the Royal Astronomical Society/Blackwell Science L<sup>A</sup>T<sub>E</sub>X style file.